Journal of Fluorine Chemistry 130 (2009) 22–29

Contents lists available at ScienceDirect

Journal of Fluorine Chemistry

journal homepage: www.elsevier.com/locate/fluor

Thermodynamic properties and phase diagrams of fluoride salts for nuclear applications

O. Beneš *, R.J.M. Konings

European Commission, Joint Research Centre, Institute for Transuranium Elements, P.O. Box 2340, 76125 Karlsruhe, Germany

ARTICLE INFO

Article history:
Received 28 February 2008
Received in revised form 19 June 2008
Accepted 3 July 2008
Available online 23 July 2008

Keywords:
Fluoride salts
Molten Salt Reactor
Thermal properties

ABSTRACT

This work is a critical review of the chemical–physical properties of the fluoride salts of interest in the Molten Salt Reactor project. In total five salt compositions are discussed. Two of them are choices for coolant applications (based on LiF–BeF_2 and NaF–$NaBF_4$ systems) one is considered as a heat transfer salt (LiF–NaF–KF system) whereas the other two are the main candidates for the fuels in non-moderated breeder and thermal breeder reactors, respectively (LiF–ThF_4 and LiF–BeF_2–ThF_4 systems). For all the systems the phase diagrams are presented with the emphasis on the melting behaviour and the vapour pressure. Heat capacity, density, viscosity and thermal conductivity, as well as the solubility for actinides in case of the fuels are presented also.

1. Introduction

In a Molten Salt Reactor the nuclear fuel is dissolved in an inorganic liquid that is pumped at a low pressure through the reactor vessel and the primary circuit and thus also serves as the primary coolant. The heat generated by the fission process is transferred to a secondary coolant in a heat exchanger. This secondary coolant is generally a molten salt also.

The first proposal for a Molten Salt Reactor dates from the 1940s when Bettis and Briant proposed it for aircraft propulsion [1]. A substantial research programme was started at Oak Ridge National Laboratory (ORNL) in the USA to develop this idea, culminating in the Aircraft Reactor Experiment (ARE) that was critical during several days in 1954. For ARE a mixture of NaF–ZrF_4 was used as carrier of the fissile UF_4 for the following reasons [2,3]:

- Wide range of solubility for thorium and uranium.
- Thermodynamic stability up to high temperatures.
- Stability to radiation (no radiolytic decomposition).
- Low vapour pressure at the operating temperature of the reactor.
- Compatibility with nickel-based alloys (Ni–Mo–Cr–Fe) that can be used as structural materials (Hastelloy).

In the second half of the 1950s the molten salt technology was transferred to the civilian nuclear programme of the US. At that time many reactor concepts were being studied and the interest in breeder reactors was large. It was recognized that the Molten Salt Reactor would be ideal for thermal breeding of uranium from thorium [1] and the Molten Salt Reactor Experiment (MSRE) was started at ORNL to demonstrate the operability of Molten Salt Reactors. Because of the breeding aspect, the neutron economy in the reactor was considered of key importance and ^{7}LiF–BeF_2 (FLIBE), with 5% ZrF_4 as oxygen getter, was selected as fuel carrier because of the very low neutron-capture cross sections of ^{7}Li ($\sigma_{thermal} = 0.045$ barn) and Be ($\sigma_{thermal} = 0.0088$ barn). The MSRE was a graphite-moderated reactor of 8 MWth that operated from 1965 to 1969. Three different fissile sources were used: $^{235}UF_4$, $^{233}UF_4$ and $^{239}PuF_3$. FLIBE was used as coolant in the secondary circuit. The results of MSRE, which have been reported in great detail [4], revealed that the selected materials (fuel, structurals) all behaved well and that the equipment behaved reliably. In that respect it was very successful.

After the MSRE a design for a prototype Molten Salt Breeder Reactor (MSBR) was made by ORNL early 1970s [5], in which a continuous reprocessing of the fuel was foreseen to reduce the neutron loss by capture in fission products. The program was stopped in 1976, in favor of the liquid metal cooled fast reactor [1] although the technology was considered promising, but recognizing the technological problems that had to be solved. The MSBR design was a 2250 MWth reactor, optimized to breed ^{233}U from thorium in a single fluid system. Online pyrochemical reprocessing was planned to clean the fuel solvent from the neutron absorbing fission products. Nevertheless interruption of reactor operation was planned every four years to replace the graphite moderator, as experiments had revealed significant swelling of graphite due to radiation damage. Because of the online clean up of the fuel, the

* Corresponding author. Tel.: +49 7247 951263; fax: +49 724 7951 198.
E-mail address: ondrej.benes@ec.europa.eu (O. Beneš).

0022-1139/$ – see front matter © 2008 Elsevier B.V. All rights reserved.
doi:10.1016/j.jfluchem.2008.07.014

zirconium addition to the fuel was not necessary and FLIBE could be used as carrier of the fertile (ThF_4) and fissile elements (UF_4). As secondary coolant a NaF–$NaBF_4$ (8–92 mol%) mixture was foreseen because the tritium retention of this salt is much better than FLIBE.

In the 1990s renewed interest in molten salt technology originated from programs looking into possibilities for transmutation of actinides. The absence of complicated fuel and fuel pin fabrication and the compatibility with pyrochemical processing in the molten salt fuel cycle were recognized as important advantages compared to conventional pellet fuel types when addressing transmutation of minor actinides. Also the interest in the use of thorium as a nuclear fuel maintained the interest in Molten Salt Reactors. As a result the MSR is now one of the six reactor concepts selected for the Generation IV initiative, that is looking at the next generation nuclear reactors. Current MSR designs, however, move away from thermal graphite moderated concepts, and favor non-moderated concepts that have a fast(er) neutron spectrum. The fuel selection is more flexible for the non-moderated reactor concepts, and other elements than ^7Li and be can be considered. One reason is that the neutron capture cross section of the alkali halides and alkali earth halides is generally lower in the 'fast' spectrum than in the thermal spectrum and also the neutron economy is not as sensitive in the 'fast' spectrum compared to the thermal one. Therefore compounds like NaF, KF, RbF or CaF_2 can be considered as part of the fuel matrix. Moreover there are some 'fast' MSR concepts [6] that are based on the chloride matrix (^{35}Cl: $\sigma_{fast} = 0.0011$ barn, whereas $\sigma_{thermal} = 43.63$ barn).

In parallel to the fuel application, molten salts have also been proposed as coolants for solid fuel reactors (fast reactors, high temperature reactors) combining their good heat transfer properties with their transparency. Table 1 gives an overview of the various application currently under investigation. It is clear that fluoride salts are very prominent, especially for applications in thermal reactors.

In this study all the fluoride systems from the primary choices in Table 1 except the LiF–NaF–BeF_2–AnF_3 system are discussed with the emphasis on their thermal properties. The LiF–NaF–BeF_2–AnF_3 system has been excluded from this study due to the lack of the experimental data. Further measurements and modelling is required here. However the first suggestion for a specific fuel composition can be found in the study by Ignatiev et al. [7]. The knowledge of the thermal properties is very important for the assessment of the feasibility of the various nuclear applications of molten salts. As discussed, a distinction must be made for fuel salts and coolant salts, although many common aspects can be identified. In general one can group the properties in (a) melting temperature, (b) physico-chemical properties, and (c) actinide solubility.

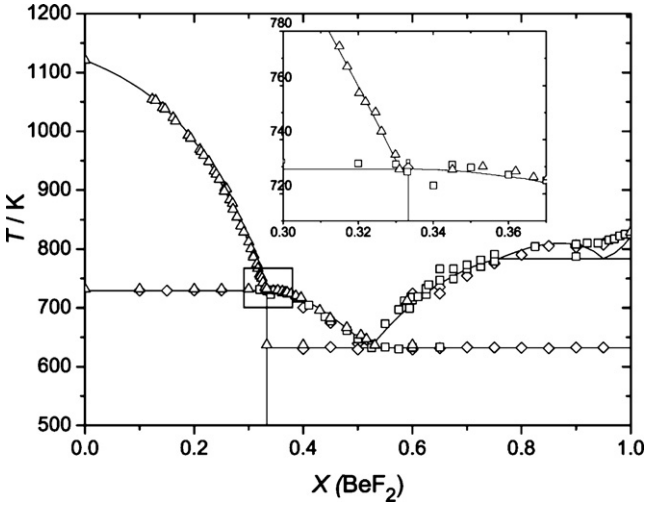

Fig. 1. The LiF–BeF_2 phase diagram after [17].

2. Fluoride salts as coolants

2.1. LiF–BeF_2

2.1.1. Phase diagram

The LiF–BeF_2 equilibrium diagram has been studied extensively by thermal analysis techniques [8–14]. The early studies generally agree on the overall shape of the system, but differences exists in the details, probably due to oxygen impurities in the salts. Thoma et al. [13] and subsequently Romberger et al. [14] established definitely the phase relations in this system. The system shows two mixed compounds: Li_2BeF_4 which melts congruently and $LiBeF_3$ which peritectically decomposes to Li_2BeF_4 and BeF_2. In addition two eutectic points were found, see Fig. 1. Vallet and Braunstein [15] suggested that a miscibility gap may occur at the BeF_2-rich side of the diagram, based on model calculations. Van der Meer et al. [16,17] arrived at the same conclusion based on optimization of the phase diagram data. The assessed phase diagram from that latter study is shown in Fig. 1.

Although the lowest melting temperature ($T = 638$ K) corresponds to $X(BeF_2) = 0.52$ the attention has been focused on the Li_2BeF_4 composition for reactor coolants, principally due to its more favorable properties. The melting point for this 66:34 composition is 732.3 K, measured experimentally [13], as compared to 728.7 K derived from the thermodynamic model.

Table 1
The various applications of molten salts in nuclear reactor science

Reactor type	Neutron spectrum	Application	Primary choice	Alternative(s)
MSR Breeder	Thermal	Fuel	^{7}LiF–BeF_2–AnF_4	
	Fast	Fuel	^{7}LiF–AnF_4	^{7}LiF–CaF_2–AnF_4
		Secondary coolant	NaF–$NaBF_4$	LiF–BeF_2, KF–KBF_4
MSR Burner	Fast	Fuel	LiF–NaF–BeF_2–AnF_3	LiF–NaF–KF–AnF_3, LiF–NaF–RbF–AnF_3
AHTR [a]	Thermal	Primary coolant	^{7}LiF–BeF_2	
VHTR [b]	Thermal	Heat transfer [e]	LiF–NaF–KF	LiCl–KCl–$MgCl_2$
MS–FR [c]	Fast	Primary coolant	LiCl–NaCl–$MgCl_2$	
SFR [d]	Fast	Intermediate coolant [f]	$NaNO_3$–KNO_3	

[a] Advanced High Temperature Reactor, Generation IV concept, thermal reactor.
[b] Very High Temperature Reactor, Generation IV concept, graphite moderated, gas cooled reactor.
[c] Molten Salt cooled Fast Reactor, Generation IV concept of the fast reactor with MS as a coolant.
[d] Sodium cooled Fast Reactor, Generation IV concept with molten sodium as a coolant.
[e] Heat transfer salt is a medium that will be used to deliver the heat from the reactor to the hydrogen production plant.
[f] to separate the sodium and the steam circuits.

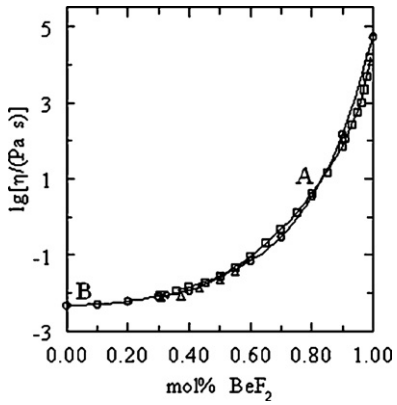

Fig. 2. The viscosity (left) and the excess molar viscosity (right) of liquid LiF–BeF_2 at 873 K; (▽) Cohen and Jones [21]; (△) Blanke et al. [18]; (□) curve A, Cantor et al. [19]; (◯) curve B, Desyatnik et al. [23]; (◇) Abe et al. [22].

2.1.2. Density and viscosity

The density of liquid LiF–BeF_2 has been measured by Blanke et al. [18] from 0 to 55 mol% BeF_2, Cantor et al. [19] for 50.2, 74.9 and 89.2 mol% BeF_2, and Cantor [20] for the 34 mol% BeF_2 composition. As discussed by van der Meer and Konings [17] the molar volume derived from the measured density data indicate ideal behavior, suggesting that the density can be interpolated from the molar volume data for the pure components. However, the density and molar volume of liquid BeF_2 are not known well, and only at a single temperature ($T = 1073$ K) and not at all as function of temperature. Therefore we have selected the results the 66:34 composition from [20]:

$$\rho\ (\mathrm{kg\,m^{-3}}) = 2146.3 - 0.4884T\ (\mathrm{K}) \tag{1}$$

The viscosity of liquid LiF–BeF_2 has been measured by Cohen and Jones [21] and Abe et al. [22] for the compositions (31 and 32.8 mol% BeF_2, respectively) as well as Blanke et al. [18], Cantor et al. [19] and Desyatnik et al. [23] for a wide(r) range of compositions and temperatures. The agreement between the studies is excellent as is shown in Fig. 2 in a isothermal section at 873 K. From the results we interpolate for the 66:34 composition:

$$\eta\ (\mathrm{mPa\,s}) = 0.116 \exp\left(\frac{3755}{T\ (\mathrm{K})}\right) \tag{2}$$

2.1.3. Heat capacity and thermal conductivity

The heat capacity of liquid LiF–BeF_2 (66–34 mol%) has been measured by Hofman and Cooke (as cited in [24]) and Douglas and Payne [25] who obtained 2.41 J K^{-1} g^{-1} (unknown temperature range) and 2.37 J K^{-1} g^{-1} (773–873 K), respectively. The value C_p (LiF–BeF_2 (66:34)) = 2.39 J K^{-1} g^{-1} has been selected.

The thermal conductivity of LiF–BeF_2 (66–34 mol%) has been measured by Cooke (as reported in [24]) to be 1.0 W m^{-1} K^{-1}, independent of the temperature. Somewhat later Cooke et al. [26] reported more detailed results, indicating that the thermal conductivity slightly increases from $\lambda = 1.0$ W m^{-1} K^{-1} at 923 K, to about 1.2 W m^{-1} K^{-1} between 1023 K and 1133 K. Kato et al. [27] measured the thermal diffusivity of the compositions 66–34 and 53–47 mol%. From their results we calculate 1.1 W m^{-1} K^{-1} for the 66–34 mol% composition, which is in good agreement with Cooke's results, and we recommend λ(LiF–BeF_2 (66–34)) = 1.1 W m^{-1} K^{-1}.

2.1.4. Vapour pressure

According to our thermodynamic data the vapour pressure of the LiF–BeF_2 (66–34 mol%) composition has been calculated for the temperature range between 823 K and 1473 K, which covers a typical operating temperature range of the Molten Salt Reactor (exact temperatures will depend on the concept, but it will most likely be in between these values) and also describes the vapour pressure at high temperature in order to simulate the fuel behaviour during the accidental conditions. The result is given in equation below:

$$\log_{10} p\ (\mathrm{Pa}) = 11.914 - \frac{13003}{T\ (\mathrm{K})} \tag{3}$$

2.2. LiF–NaF–KF

2.2.1. Phase diagram

The LiF–NaF–KF phase diagram has been measured by Bergman and Dergunov [28]. It is characterized by one eutectic invariant point that was experimentally determined by Bergman and Dergunov at $T = 727$ K and LiF–NaF–KF (46.5–11.5–42.0 mol%). This temperature was confirmed by new differential scanning calorimetric measurements at our institute. This eutectic composition is generally considered for coolant applications.

The thermodynamic assessment of this system has been made in several studies [29–31]. In all cases very good agreement between the calculated phase diagram and the experimental data has been achieved. The modelled phase diagram is shown in Fig. 3 as a liquidus projection. The calculated eutectic, $T = 726$ K and LiF–NaF–KF (45.3–13.2–41.5 mol%) [31], in good agreement with the experimental value.

2.2.2. Density and viscosity

The density of the eutectic melt of the LiF–NaF–KF system has been measured by Chrenkova et al. [32] for the temperature range 940–1170 K. The exact composition of the LiF–NaF–KF melt measured in their study was $X_{LiF} = 0.465$, $X_{NaF} = 0.115$, $X_{KF} = 0.420$, thus corresponding to the eutectic composition as found by Bergman and Dergunov [28]. The density as a function of temperature of the eutectic composition has also been reported by Powers et al. [33] for an unspecified temperature range. As shown in Fig. 4 the data by Chrenkova et al. and by Powers et al. differ significantly. The results of Chrenkova et al. are close to the density calculated assuming ideal behaviour and the curve has almost the

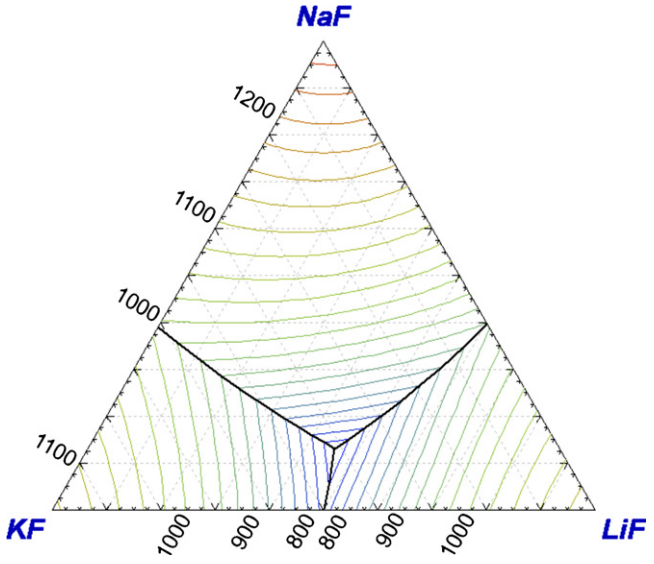

Fig. 3. Calculated liquid surface of the LiF–NaF–KF phase diagram after [31]. Isotherms are labelled in K with interval of 25 K.

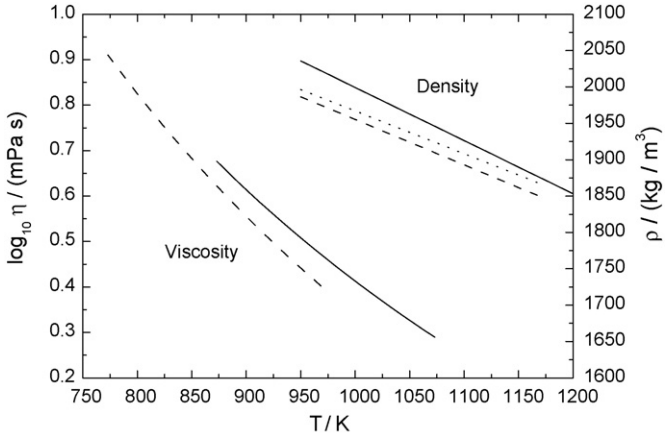

Fig. 4. Viscosity and density functions of temperature reported by Chrenkova et al. (dashed line) and Powers et al. (solid line). For comparison the ideal density behavior is represented by a dotted line.

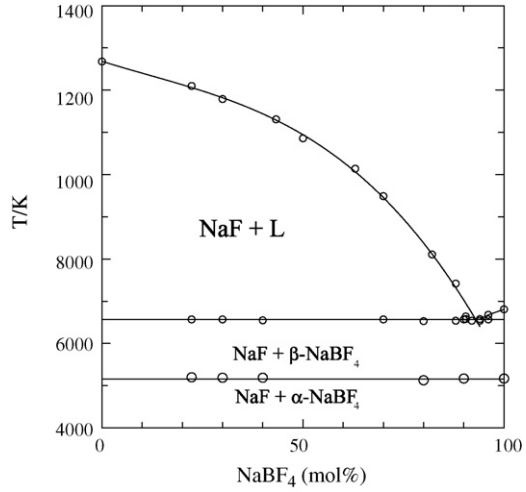

Fig. 5. The equilibrium diagram of the NaF–$NaBF_4$ system after Barton et al. [36].

same slope which is consistent with our observations that most of these fluoride systems are ideal. For that reason we recommend the data by Chrenkova et al.:

$$\rho\ (\mathrm{kg\,m^{-3}}) = 2579.3 - 0.6240T\ (\mathrm{K}) \quad (4)$$

The viscosity of the eutectic melt of the LiF–NaF–KF system has been measured by Chrenkova et al. [32] for the temperature range 773–973 K and by Powers at al. [33] for the temperature range 873–1073 K. The comparison between the data by Chrenkova et al. and by Powers et al. is shown in Fig. 4. The data by Chrenkova et al. have been selected:

$$\log_{10}\eta\ (\mathrm{mPa\,s}) = -1.6044 + \frac{1944}{T\ (\mathrm{K})} \quad (5)$$

2.2.3. Heat capacity and thermal conductivity

Powers et al. [33] reported the heat capacity of the LiF–NaF–KF (46.5–11.5–42) melt measured at $T = 973$ K, giving $C_p = 1.88\ \mathrm{J\,g^{-1}\,K^{-1}}$. This value is significantly higher from the ideal behavior ($C_{p,\mathrm{ideal}} = 1.66\ \mathrm{J\,g^{-1}\,K^{-1}}$).

The same authors measured the thermal conductivity of the eutectic composition, giving $\lambda = 4.5\ \mathrm{W\,m^{-1}\,K^{-1}}$. This value is much higher than the measurement (773–1173 K) by Ewing et al., $\lambda = 0.6\ \mathrm{W\,m^{-1}\,K^{-1}}$. Smirnov et al. [34] measured the thermal conductivity of eutectic LiF–NaF–KF (46.5–11.5–42 mol%) from 790 K to 1080 K and obtained $\lambda = 0.36 + 5.6 \times 10^{-4}\,T$ (K) $\mathrm{W\,m^{-1}\,K^{-1}}$, giving $0.8\ \mathrm{W\,m^{-1}\,K^{-1}}$ at $T = 773$ K. Kato et al. [27] measured the thermal diffusivity of LiF–NaF–KF (46.5–11.5–42 mol%) in the temperature range 730–823 K and obtained $a = 7.6 \times 10^{-4} + 6.3 \times 10^{-7}\,T\ \mathrm{K\,m^2\,h^{-1}}$, which yields $0.8\ \mathrm{W\,m^{-1}\,K^{-1}}$ at $T = 773$ K when combined with the selected heat capacity and density values. We thus recommend:

$$\lambda\ (\mathrm{W\,m^{-1}\,K^{-1}}) = 0.36 + 5.6 \times 10^{-4}T\ (\mathrm{K}) \quad (6)$$

2.2.4. Vapour pressure

Based on our thermodynamic assessment the vapour pressure of the LiF–NaF–KF (46.5–11.5–42 mol%) composition has been calculated for the temperature range between 823 K and 1473 K. The result is given by the equation below:

$$\log_{10} p\ (\mathrm{Pa}) = 10.748 - \frac{10789}{T\ (\mathrm{K})} \quad (7)$$

2.3. NaF–$NaBF_4$

2.3.1. Phase diagram

The equilibrium diagram of the NaF–$NaBF_4$ system has been studied by Selivanov and Stender [35] and Barton et al. [36]. Both studies indicate that it is a simple eutectic system, but the eutectic temperatures and compositions differ considerably. In view of their more careful sample preparation, the results of Barton et al. are preferred, and this diagram is shown in Fig. 5. They found $x_{\mathrm{eut}} = (92 \pm 1)$ mol% $NaBF_4$ with $T_{\mathrm{eut}} = (657 \pm 1)$ K.

Pure molten $NaBF_4$ is not suited as coolant since it has a relatively high partial pressure of BF_3 gas. Therefore the eutectic composition is the reference in this system.

2.3.2. Density and viscosity

The density of NaF–$NaBF_4$ (8–92) was measured by Cantor [20] from 673 K to 864 K. The results can be represented by the equation:

$$\rho\ (\mathrm{kg\,m^{-3}}) = 2446.3 - 0.711T\ (\mathrm{K}) \quad (8)$$

The viscosity of NaF–$NaBF_4$ (8–92) was measured by Cantor [20] from 682 K to 810 K. The results can be represented by the equation:

$$\eta\ (\mathrm{mPa\,s}) = 0.0877 \exp\left(\frac{2240}{T\ (\mathrm{K})}\right) \quad (9)$$

2.3.3. Heat capacity and thermal conductivity

The heat capacity of the NaF–$NaBF_4$ (8–92 mol%) melt has been determined by Dworkin (as a reference in [20]) as $C_p = 1506\ \mathrm{J\,kg^{-1}\,K^{-1}}$.

The thermal conductivity of the NaF–$NaBF_4$ (8–92 mol%) melt has been reported by Cooke et al. [26] for temperature range 740–1000 K. However they reported their results in graphical form only without listing the exact values or equations. Thus their data have been obtained by digital subtraction from the figure and the temperature function of the thermal conductivity has been determined by linear fit, giving:

$$\lambda\ (\mathrm{W\,m^{-1}\,K^{-1}}) = 0.66 - 2.37\,10^{-4}T\ (\mathrm{K}) \quad (10)$$

It is interesting to compare these results with those of Cantor et al. [24] who reported preliminary measurements of the thermal conductivity of pure liquid $NaBF_4$, finding $\lambda = 0.51\ \mathrm{W\,m^{-1}\,K^{-1}}$,

Table 2
Selected properties of coolant salts

Property	LiF–BeF_2 (0.66–0.34)	NaF–$NaBF_4$ (0.08–0.92)	LiF–NaF–KF (0.465–0.115–0.42)
Melting point (K)	728	657 ± 1	727
ρ (kg m^{-3})	$2146.3 - 0.4884T$ (K)	$2446.3 - 0.711T$ (K)	$2579.3 - 0.6240T$ (K)
η (mPa s)	$1.81 \exp(1912.2/T$ (K))	$0.0877 \exp(2240/T$ (K))	$-1.6044 + (1944/T$ (K))
C_p (J K^{-1} g^{-1})	2.39	1.50	1.883
λ (W m^{-1} K^{-1})	1.1	$0.66 - 2.37 \times 10^{-4}T$ (K)	0.8
$\log_{10} p$ (Pa)	$11.914 - (13003/T$ (K))	$11.638 - (6550.6/T$ (K))	$11.042 - (11063/T$ (K))

Table 3
Selected properties of fuel salts

Property	LiF–ThF_4 (0.78–0.22)	LiF–BeF_2–ThF_4 (0.717–0.16–0.123)
Melting point (K)	841	771
ρ (kg m^{-3})	$5543.0 - 1.2500T$ (K)	$4124.3 - 0.8690T$ (K)
η (mPa s)	$0.365 \exp(2735/T$ (K))	$0.062 \exp(4636/T$ (K))
C_p (J K^{-1} g^{-1})	1.000	1.230
λ (W m^{-1} K^{-1})	$\sim$1.5	1.51
$\log_{10} p$ (Pa)	$11.902 - (12989/T$ (K))	$11.158 - (10790.5/T$ (K))

thus on average slightly higher than the NaF–$NaBF_4$ (8–92) eutectic composition.

2.3.4. Vapour pressure

The vapour pressure of BF_3 in the NaF–$NaBF_4$ system has been measured by Cantor et al. [37]. They measured the equilibrium of the BF_3 gaseous species over the melt for the composition range of 5–100 mol% $NaBF_4$ and the temperature range of 698–1473 K. However in their report they 'only' show the results for 900 K, 1000 K and 1100 K. Based on this triplet of data the vapour pressure equation of NaF–$NaBF_4$ (8–92 mol%) has been determined, giving:

$$\log_{10} p \ (\text{Pa}) = 11.638 - \frac{6550.6}{T \ (\text{K})} \tag{11}$$

The selected properties of all coolant salts considered in this study are summarized in Table 2.

3. Fluoride salts as fuel carrier

3.1. LiF–AnF_4

3.1.1. Phase diagram

The equilibrium diagrams of the LiF–ThF_4 system was reported by Thoma et al. [38] based on thermal analysis and thermal quenching. The phase diagram has been thermodynamically assessed by van der Meer et al. [39] based on these data and is shown in Fig. 6. The LiF–ThF_4 phase diagram consists of four mixed compounds: Li_3ThF_7, which melts congruently and $LiThF_4$, $LiTh_2F_9$ and $LiTh_4F_{17}$, all melting peritectically. Two eutectic points were found at $x_{eut_1} = (22.4 \pm 1)$ mol% ThF_4 with $T_{eut_1} = (841 \pm 1)$ K and $x_{eut_2} = (28.3 \pm 1)$ mol% ThF_4 with $T_{eut_2} = (838 \pm 1)$ K, respectively.

The solubility of ThF_4 in the matrix of LiF can be deduced from the binary phase diagram. For example the solubility of ThF_4 in the melt of LiF for $T = 903$ K (inlet temperature of the Thorium Molten Salt Reactor) is between 20.0 and 32.3 mol%. Compositions in this range are thus of interest as fuel for a non-moderated Thorium Molten Salt Reactor. In practice the LiF–ThF_4 (78–22 mol%) composition is the prime choice.

In this concept AnF_4 is represented mainly by ThF_4 which serves as a fertile material and by UF_4 which is the fissile material, normally up to 4 mol%. Since UF_4 and ThF_4 form close to ideal solid and liquid solutions, the melting point of the fuel is negligibly affected by the UF_4/ThF_4 substitution. The effect of the UF_4 addition is demonstrated in the inset graph of Fig. 6 which shows the calculated liquidus line (the very upper line) of the ThF_4–UF_4 pseudobinary system with constant amount of LiF at 78 mol%. The left axis of the graph corresponds to the proposed LiF–ThF_4 (78–22.4 mol%) composition (eutectic$_1$ of the LiF–ThF_4 system) and the right axis corresponds to the LiF–UF_4 (78–22.4 mol%) composition, thus in that case all ThF_4 is substituted by UF_4. As can be seen from the figure the liquidus line along this section is nearly constant with total increase of only 4 K.

3.1.2. Density and viscosity

The density of LiF–ThF_4 mixtures was measured by Porter and Meaker [40] and Hill et al. [41]. The data are in good agreement and clearly indicate a linear dependence of the molar volume with composition, confirming ideal behaviour. The density of the 78–22 composition as measured by Porter and Meaker [40] is given by

$$\rho \ (\text{kg m}^{-3}) = 5543 - 1.25T \ (\text{K}) \tag{12}$$

The viscosity of LiF–ThF_4 mixtures was measured by Chervinskij et al. [42] from 0 to 100 mol% ThF_4. The results reveal a strong positive deviation from ideal behaviour around the eutectic composition. An isothermal section is shown in Fig. 7, which shows a steady increase from LiF to ThF_4. The viscosity of the 78–22 composition interpolated from the results is given by

$$\eta \ (\text{mPa s}) = 0.365 \exp\left(\frac{2735}{T \ (\text{K})}\right) \tag{13}$$

The viscosity of the LiF–UF_4 system measured by the same group [43] shows a less strong increase with the AnF_4 content compared

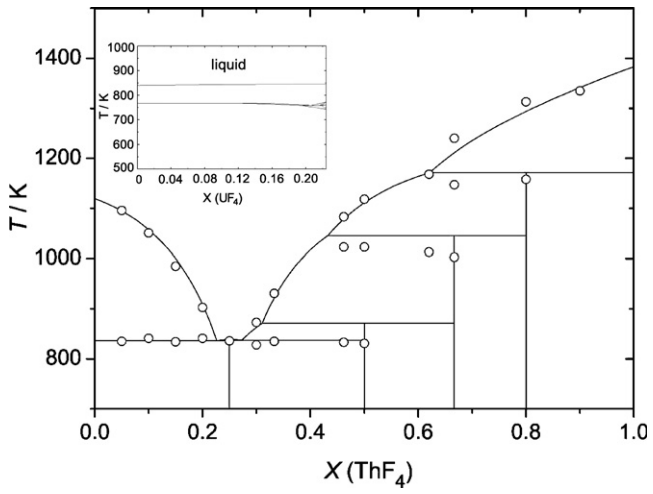

Fig. 6. The equilibrium diagram of the LiF–ThF_4 system assessed in [39]. Experimental data points are from [38]. Inset: calculated ThF_4–UF_4 pseudobinary system with constant amount of LiF at 78 mol%.

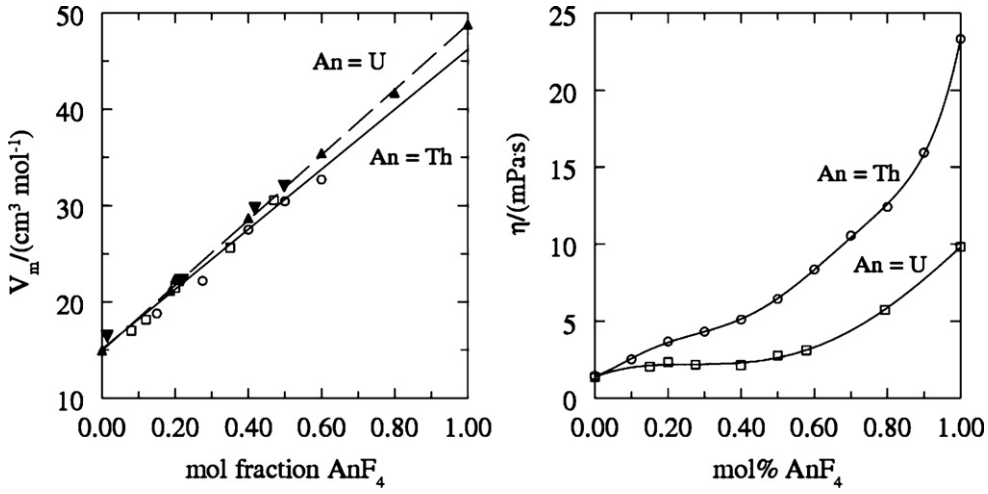

Fig. 7. The molar volume (left) and viscosity (right) of liquid LiF–ThF_4 and LiF–UF_4 at 1273 K.

to ThF_4 (Fig. 7). As a result the above equation probably slightly overestimates the viscosity in case of partly replacement of ThF_4 by UF_4.

3.1.3. Heat capacity and thermal conductivity

To our best knowledge none of these properties has been measured for the LiF–ThF_4 system. We have estimated the heat capacity of the LiF–ThF_4 (78–22 mol%) composition based on the comparison between the ideal heat capacity and the measured data from other fluoride systems taken from [33]. An average positive deviation from the ideal behaviour has been found to be 11%. If we combine this difference with the ideal heat capacity of the LiF–ThF_4 (78–22 mol%) composition, we obtain our suggested value: $C_p = 1000\ \mathrm{J\ kg^{-1}\ K^{-1}}$. There are not enough data to accurately estimate the thermal conductivity of the LiF–ThF_4 (78–22 mol%) composition, however we suggest the value to be slightly higher than the value of the LiF–BeF_2 (66–34 mol%) and close to the value for LiF–BeF_2–ThF_4 (71.7–16–12.3 mol%) compositions, thus $\lambda = \sim 1.5\ \mathrm{W\ m^{-1}\ K^{-1}}$ (see Section 3.2.4).

3.1.4. Vapour pressure

According to the thermodynamic data obtained from [44] the vapour pressure of the LiF–ThF_4 (78–22 mol%) composition has been calculated for the temperature range between 839 K to 1473 K. The result is given in equation below:

$$\log_{10} p\ (\mathrm{Pa}) = 11.902 - \frac{12989}{T\ (\mathrm{K})} \qquad (14)$$

The vapour pressure of the LiF–ThF_4–UF_4 (78–18–4 mol%) composition is slightly lower compared to a system with no UF_4 content.

3.2. LiF–BeF_2–AnF_4

3.2.1. Phase diagram

The LiF–BeF_2–ThF_4 system is a reference salt for a Molten Salt Reactor when designed as a thermal breeder. The equilibrium diagram of this system was measured by Thoma et al. [45]. It contains a single eutectic at 1.5 mol% ThF_4 and $T_{eut} = (629 \pm 3)$ K; no ternary compounds were found. van der Meer et al. [44] calculated the ternary from the assessed binaries and found an excellent agreement with the experimental diagram. The calculated phase diagram of the LiF–BeF_2–ThF_4 system is shown in Fig. 8 as a projection of the liquidus surface.

In the MSBR concept the proposed fuel composition in the LiF–BeF_2–AnF_4 system was 71.7–16.0–12.3, where the AnF_4 fraction was made up of 12.0 mol% for ThF_4 and 0.3 mol% for UF_4. In this section the AnF_4 is represented by pure ThF_4 what is possible for the same reasons as discussed in the Section 3.1.1. If we then assume that the concentration of ThF_4 must be 12.3 mol%, it is possible, according to our thermodynamic data, to determine the lowest melting temperature of such a system and its exact composition. It has been found at $T = 786$ K and LiF–BeF_2–ThF_4 (67.1–20.6–12.3 mol%) (Composition 1), thus reasonably close to the data of the MSBR fuel ($T = 771$ K and LiF–BeF_2–AnF_4 (71.7–16.0–12.3 mol%) (Composition 2)). This means that keeping the safety margin of 50 K the inlet temperature of the reactor must be minimum 836 K. It is a promising result because it is lower than the inlet temperature in MSBR which was 839 K. According to the modeled phase diagram (Fig. 8) the calculated liquidus temperature of the MSBR composition (Composition 2) is 795 K.

Since the melting temperatures of the Compositions 1 and 2 are very close, we will focus the discussion only on preferred composition of the MSBR concept(LiF–BeF_2–ThF_4 (71.7–16.0–12.3 mol%) (Composition 2). This salt has also been more extensively studied, thus more properties are known.

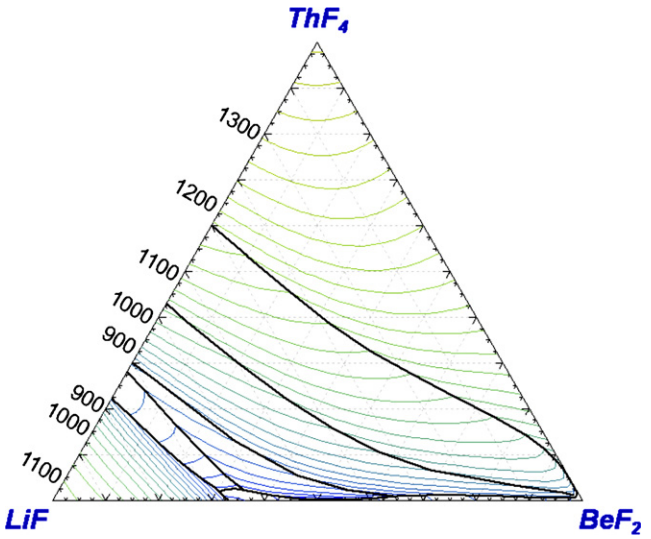

Fig. 8. Calculated liquid surface of the LiF–BeF_2–ThF_4 phase diagram. Isotherms are labeled in K with interval of 25 K.

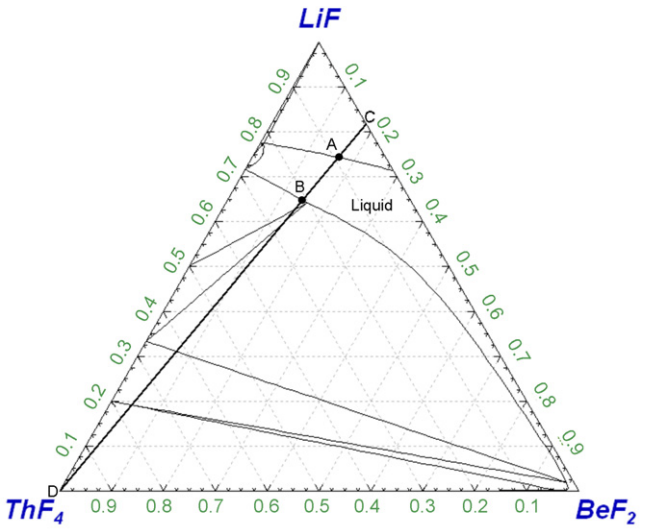

Fig. 9. Isothermal plot of the LiF–BeF_2–ThF_4 phase diagram at $T = 839$ K.

3.2.2. Solubility of ThF_4 in the LiF–BeF_2 melt

The solubility of ThF_4 in the LiF–BeF_2 matrix has been calculated for $T = 839$ K (inlet temperature of MSBR) keeping a constant ratio of LiF/BeF_2 = 0.818/0.182. This ratio corresponds to the fuel composition proposed in MSBR. Fig. 9 shows the ternary phase diagram of the LiF–BeF_2–ThF_4 system at $T = 839$ K. The straight bold line represents the LiF/BeF_2 ratio at 0.818/0.182 within the whole field of the diagram, while the ThF_4 concentration varies from 0 to 100 mol% when moving from point "C" towards "D". The solubility of ThF_4 in the LiF–BeF_2 matrix thus derived is between 9.2 and 20.8 mol%. The interval of the solubility is represented by the "A" and "B" signs, respectively which correspond to the intersection of the "CD" line with the surface of the liquid field.

3.2.3. Density and viscosity

The density of three compositions from the LiF–BeF_2–ThF_4 system with almost constant LiF concentration were measured by Cantor [20]. Unfortunately the density of the LiF–BeF_2–ThF_4 (71.7–16.0–12.3) composition has not been measured, however very close composition (LiF–BeF_2–ThF_4 (70.06–17.96–11.98)) has been determined and the corresponding density function is given below:

$$\rho\ (\mathrm{kg\,m^{-3}}) = 4043.9 - 0.8064T\ (\mathrm{K}) \quad (15)$$

It has been shown in the previous study by van der Meer et al. [46] that the molar volumes and thus the densities of all three LiF–BeF_2–ThF_4 compositions measured in [20] behave almost ideally. Based on this triplet of data and with the assumption of the ideality it is possible to estimate the density function of temperature of pure BeF_2 which has not been measured yet. The density of liquid BeF_2 was indeed measured by MacKenzie [47], but only at 1073 K obtaining 1947 ± 10 kg m^{-3}. Cantor et al. [19] also measured the density, but due to the experimental difficulties derived only an approximate value, 1960 kg m^{-3} at 1123 K. The value of MacKenzie is recommended and taken as a constraint in our estimation. The obtained density for liquid BeF_2 as a function of temperature is shown below:

$$\rho\ (\mathrm{kg\,m^{-3}}) = 3190.5\,(\pm 58.1) - 1.1589\,(\pm 0.0468)T\ (\mathrm{K}) \quad (16)$$

Using the Eq. (16) together with the selected data for the LiF and ThF_4 densities taken from [46] we have calculated the expected density function of temperature for the LiF–BeF_2–ThF_4 (71.7–16.0–12.3) composition (MSBR). The obtained equation is given below:

$$\rho\ (\mathrm{kg\,m^{-3}}) = 4124.3 - 0.8690T\ (\mathrm{K}) \quad (17)$$

The results from Eqs. (15) and (17) agree very well. Since the former equation is based on the experimental results whereas the later one is an estimate and both equations refer to very similar compositions, it can be justified that the density in the LiF–BeF_2–ThF_4 system can be extrapolated based on the ideal behavior.

The viscosity of liquid LiF–BeF_2–ThF_4 of two compositions was measured by Cantor [20]. The viscosity of the quaternary LiF–BeF_2–ThF_4–UF_4 (71–16–12–1) composition, which is nearly identical to our reference selection (LiF–BeF_2–ThF_4 (71.7–16–12.3)), has been reported in [33] for a temperature range 873–1073 K, giving:

$$\eta\ (\mathrm{mPa\,s}) = 0.062 \exp\left(\frac{4636}{T\ (\mathrm{K})}\right) \quad (18)$$

3.2.4. Heat capacity and thermal conductivity

Araki and Kato [48] measured the thermal diffusivity of liquid LiF–BeF_2–ThF_4 (64–18–18 mol%) from which they derived the thermal conductivity, using their heat capacity data and an estimated density. The results indicate an almost constant value in the temperature range 850–1000 K: 0.95 W m^{-1} K^{-1} to 0.98 W m^{-1} K^{-1}. The recommended heat capacity according to Araki and Kato is $C_p = 1230$ J kg^{-1} K^{-1}. Both data, heat capacity and thermal conductivity, are measured for a LiF–BeF_2–ThF_4 composition that is slightly different from the LiF–BeF_2–ThF_4 composition considered in this work (71.7–16.0–12.3 mol%). Cooke et al. [26] reported (in graphical form only) the thermal conductivity of liquid LiF–BeF_2–ThF_4–UF_4 (67.5–20–12–0.5 mol%) for the temperature range 800–1150 K. The data scatter around $\lambda = 1.2$–1.4 W m^{-1} K^{-1}, with a suggested maximum at 973 K. This result is somewhat different from that by Araki and Kato [48]. Since the results for liquid LiF–BeF_2 by both groups are in good agreement, the variation probably arises from differences in BeF_2 and MF_4 content. The results from above mentioned sources [48,26] indicate that in the composition range where the measurements have been, the thermal conductivity decreases with increasing (BeF_2 + MF_4) content, where M is not only Th and U but also Zr. The LiF–BeF_2–ThF_4 (71.7–16.0–12.3 mol%) composition is just outside this range($X(BeF_2 + MF_4) = 28.3$ mol%), and linear extrapolation would suggest $\lambda = 1.51$ W m^{-1} K^{-1} at $T = 1023$ K (solid line in Fig. 10). However, such linear extrapolation would suggest a

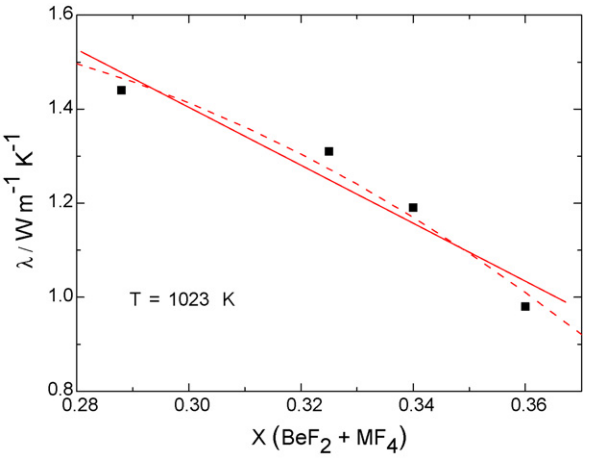

Fig. 10. Extrapolation of the thermal conductivity of the LiF–BeF_2–ThF_4 (71.7–16.0–12.3 mol%) composition at $T = 1023$ K. Solid line: linear fit; dashed line: polynomial fit.

relatively high thermal conductivity of LiF + ThF_4 (78–22 mol%). Alternatively one could extrapolate the results in a non-linear way (dashed line in Fig. 10). This would suggest $\lambda = 1.49\ W\ m^{-1}\ K^{-1}$at $T = 1023\ K$, which is very close. In this case the thermal conductivity of LiF+ThF_4 (78–22 mol%) is 1.6, which is more realistic. We recommend

$$\lambda = 1.51\ W\ m^{-1}\ K^{-1} \quad (19)$$

It must be noted that it is not possible to accurately estimate the heat capacity of the salt systems containing BeF_2 on a basis of the Neumann–Kopp rule (ideal behaviour), because the heat capacity of the pure liquid BeF_2 increases with temperature, whereas most of the fluoride mixtures have rather constant values in the liquid state. We have selected the estimated value by Araki and Kato [48] for this quantity.

3.2.5. Vapour pressure

According to our thermodynamic data the vapour pressure of the LiF–BeF_2–ThF_4 (71.7–16.0–12.3) composition has been calculated for the temperature range of 823–1473 K and the obtained result is shown in the following equation:

$$\log_{10} p\ (\mathrm{Pa}) = 11.158 - \frac{10790.5}{T\ (\mathrm{K})} \quad (20)$$

The selected properties of the LiF-ThF_4 (0.78–0.22) and the LiF-BeF_2-ThF_4 (0.717–0.16–0.123) fuel compositions are reported in Table 3.

4. Conclusion

The melting temperatures of most binary and ternary salts are reasonably well known, and reliable thermodynamic models have been developed to predict melting points of ternary and quaternary mixtures. Exceptions are salts containing transuranium actinides of relevance to burner reactors. In this field a significant effort is needed in the near future. The main needs are thus (i) measurements on plutonium and other actinide trifluorides (ii) verification measurements in ternary and quaternary systems to check and improve thermodynamic models.

Physicochemical properties (density, viscosity, heat capacity, thermal conductivity) are poorly known for most of the salts that have been identified. An exception is the ^{7}LiF–BeF_2–ThF_4–UF_4 system that was extensively studied in the 1960s. Of these properties, the density (or molar volume) follows close to ideal behaviour and can be easily obtained from the pure compounds. This is not true for the other properties, but there is generally lack accurate of data. Systematic experimental studies are needed here, especially on composition with actinides. Especially thermal conductivity is poorly known, and also theoretical models are poorly developed.

Actinide solubility is a key issue for transmutation or burner fuels, but only a limited number of studies on PuF_3 solubility exist and none on the solubility of NpF_4, AmF_3 or CmF_3. Solubility determinations are therefore of prime importance.

Acknowledgements

O.B. acknowledges the European Commission for support given in the frame of the program 'Training and Mobility of Researchers'. This work has been performed in the frame of the MOST project of the 6th Framework programme of the European Commission (contract no. FIKI-CI-2001-20183), and the ALISIA project of the 7th Framework programme of the European Commission (contract no. FI60-044809).

References

[1] H.G. MacPherson, Nucl. Sci. Eng. 90 (1985) 374.
[2] W.R. Grimes, D.R. Cuneo, C.R. Tipton Jr., Reactor Handbook, 2nd edition, Interscience Publ., New York, 1960 (Chapter 17).
[3] W.R. Grimes, Nucl. Appl. Technol. 8 (1970) 37.
[4] P.N. Haubenreich, J.R. Engel, Nucl. Appl. Technol. 8 (1970) 118–133.
[5] R.C. Robertson, Technical Report ORNL-4541, 1971.
[6] A. Mourogov, P.M. Bokov, Energy Convers. Manage. 47 (2006) 2761.
[7] V. Ignatiev, A.V. Merzlyakov, V.G. Subbotin, A.V. Panov, Yu.V. Golovatov, Atom. Energy 101 (2006) 822–829.
[8] D.M. Roy, R. Roy, E.F. Osborn, J. Am. Ceram. Soc. 33 (1950) 85–90.
[9] A.V. Novoselova, Yu.P. Simanov, Y. Yarembash, Zh. Fiz. Khim. 26 (1952) 1244–1246.
[10] D.M. Roy, R.R. Roy, E.F. Osborn, J. Am. Ceram. Soc. 36 (1953) 185–190.
[11] D.M. Roy, R.R. Roy, E.F. Osborn, J. Am. Ceram. Soc. 36 (1954) 300–305.
[12] L.V. Jones, D.E. Etter, C.R. Hudgens, A.A. Huffman, T.B. Rhinehammer, P.A. Tucker, P.A. Tucker, L.J. Wittenberg, J. Am. Ceram. Soc. 45 (1962) 79–83.
[13] R.E. Thoma, H. Insley, H.A. Friedman, G.M. Hebert, J. Nucl. Mater. 27 (1968) 166–180.
[14] K.A. Romberger, J. Braunstein, R.E. Thoma, J. Phys. Chem. 76 (1972) 1154–1159.
[15] C.E. Vallet, J. Braunstein, J. Am. Ceram. Soc. 60 (1977) 316–322.
[16] J.P.M. van der Meer, R.J.M. Konings, M. Jacobs, H.A.J. Oonk, J. Nucl. Mater. 344 (2005) 94–99.
[17] J.P.M. van der Meer, R.J.M. Konings, H.A.J. Oonk, J. Nucl. Mater. 357 (2006) 48–57.
[18] B.C. Blanke, E.N. Bousquet, M.L. Curtis, E.L. Murphy, Technical Report USAEC MLM-1086, 1956.
[19] S. Cantor, W.T. Ward, C.T. Moynihan, J. Chem. Phys. 50 (1969) 2874–2879.
[20] S. Cantor, Technical Report ORNL-TM-4308, 1971.
[21] S.I. Cohen, T.N. Jones, Technical Report ORNL-2278, 1957.
[22] Y. Abe, O. Kosugiyama, A. Nagashima, J. Nucl. Mater. 99 (1981) 173–183.
[23] V.N. Desyatnik, A.I. Nechaev, Yu.F. Chervinskii, Zh. Prikl. Khim. 54 (1981) 2310–2313.
[24] S. Cantor, J.W. Cooks, A.S. Dworkin, G.D. Robbins, R.E. Thoma, G.M. Watson, Technical Report ORNL-TM-2316, 1968.
[25] T.B. Douglas, W.H. Payne, J. Res. NBS 73A (1969) 479.
[26] J.W. Cooke, H.W. Hoffman, J.J. Keyes, Technical Report ORNL-TM-4396, February 1969.
[27] Y. Kato, K. Furukawa, N. Araki, Y. Kato, High Temp.-High Press. 15 (1983) 191–198.
[28] A.G. Bergmann, E.P. Dergunov, Dokl. Acad. Sci. URSS 31 (1941) 753.
[29] J. Sangster, A.D. Pelton, J. Phase Equilib. 12 (1991) 511.
[30] P. Chartrand, A.D. Pelton, Metall. Trans. 32A (2001) 1385.
[31] O. Beneš, R.J.M. Konings, Comput. Coupling Phase Diagrams Thermochem. 32 (2008) 121–128.
[32] M. Chrenková, V. Daněk, R. Vasiljev, A. Silný, V. Kremetsky, E. Polyakov, J. Mol. Liq. 102 (2003) 213–226.
[33] W.D. Powers, S.I. Cohen, N.D. Greene, Nucl. Sci. Eng. 71 (1963) 200–211.
[34] M.V. Smirnov, V.A. Khokhlov, E.F. Filatov, Electrochim. Acta 32 (1987) 1019–1026.
[35] V.G. Selivanov, V.V. Stender, Russ. J. Inorg. Chem. 2 (1958) 279–282.
[36] C.J. Barton, L.O. Gilpatrick, J.A. Bornmann, H.H. Stone, T.N. McVay, H. Insley, J. Inorg. Nucl. Chem. 33 (1970) 337–344.
[37] S. Cantor, C.E. Roberts, H.F. McDuffie, Technical Report ORNL-4229, December 1967.
[38] R.E. Thoma, et al. J. Am. Ceram. Soc. 42 (1959) 563.
[39] J. van der Meer, R.J.M. Konings, M.H.G. Jacobs, H.A.J. Oonk, J. Nucl. Mater. 344 (2005) 94–99.
[40] B. Porter, R.E. Meaker, Technical Report BMI RI-6836, 1966.
[41] D.G. Hill, S. Cantor, W.T. Ward, J. Inorg. Nucl. Chem. 29 (1967) 241–243.
[42] Yu.F. Chervinskii, V.N. Desyatnik, A.I. Nechaev, Zh. Fiz. Khim. 56 (1982) 1946–1949.
[43] V.N. Desyatnik, A.I. Nechaev, Yu.F. Chervinskii, Russ. J. Phys. Chem. 53 (1979) 986–988.
[44] J. van der Meer, R.J.M. Konings, H.A.J. Oonk, J. Nucl. Mater. 357 (2006) 48–57.
[45] R.E. Thoma, H. Insley, H.A. Friedman, C.F. Weaver, J. Phys. Chem. 64 (1960) 865.
[46] J. van der Meer, R.J.M. Konings, J. Nucl. Mater. 360 (2007) 16–24.
[47] J.D. Mackenzie, J. Phys. Chem. 64 (1960) 306–309.
[48] N. Araki, Y. Kato, in: T. Shibata, K. Kanda (Eds.), Research on Thorium Fuel, Ministry of Education, Science and Culture, Tokyo, Japan, 1987, pp. 83–86.